Medial to lateral frontal functional connectivity mapping reveals the organization of cingulate cortex

Marion Ducret, Camille Giacometti, Manon Dirheimer, Audrey Dureux, Delphine Autran-Clavagnier, Fadila Hadj-Bouziane, Charles Verstraete, Franck Lamberton, Charles Wilson, Céline Amiez, et al.

Medial to lateral frontal functional connectivity mapping reveals the organization of cingulate cortex

Authors: Ducret Marion[1], Giacometti Camille[1], Dirheimer Manon[2], Dureux Audrey[2], Autran-Clavagnier Delphine[3], Hadj-Bouziane Fadila[2], Verstraete Charles[1,4], Lamberton Frank [5,6], Wilson Charles R.E.[1], Amiez Céline[1*], Procyk Emmanuel[1*]

[1] Université Lyon 1, Inserm, Stem Cell and Brain Research Institute, INSERM U1208, 69500 Bron, France.
[2] Integrative Multisensory Perception Action and Cognition Team (ImpAct), INSERM U1028, CNRS UMR5292, Lyon Neuroscience Research Center (CRNL), Lyon, France; University of Lyon 1, Lyon, France.
[3] Inovarion, 75005 Paris, France
[4] Institut de neuromodulation, GHU Paris psychiatrie et neurosciences, Centre Hospitalier Sainte-Anne, pôle hospitalo-universitaire 15, Université Paris Cité, Paris, France
[5] CERMEP-Imaging Platform, Bron, France.
[6] SFR Lyon-Est, Université Lyon 1, CNRS UAR3453, INSERM US7, U69500, Lyon, France.
* The authors contributed equally to the article

Corresponding authors : marion.ducret@inserm.fr ; celine.amiez@inserm.fr ; emmanuel.procyk@inserm.fr

Abstract

The functional organization of the frontal lobe is a source of debate, focusing on broad functional subdivisions, large-scale networks, or local refined specificities. Multiple neurocognitive models have tried to explain how functional interactions between cingulate and lateral frontal regions contribute to decision making and cognitive control, but their neuroanatomical bases remain unclear. We provide a detailed description of the functional connectivity (FC) between cingulate and lateral frontal regions using resting-state functional MRI in rhesus macaques. The analysis focuses on the FC of the rostral part of the cingulate sulcus with the lateral frontal cortex. Data-driven and seed-based analysis revealed 3 clusters within the cingulate sulcus organized along the rostro-caudal axis: the anterior, mid, and posterior cluster display increased FC with, respectively, the anterior lateral prefrontal regions, face-eye lateral frontal motor cortical areas, and hand lateral frontal motor cortex. The location of these clusters can be predicted in individual subjects thanks to morphological landmarks. These results suggest that the anterior cluster corresponds to the anterior cingulate cortex, whereas the posterior clusters correspond to the face-eye and hand cingulate motor areas within the anterior midcingulate cortex. These data provide a comprehensive framework to identify cingulate subregions based on FC and local organization.

Citation: Ducret M, Giacometti C, Dirheimer M, Dureux A, Autran-Clavagnier D, Hadj-Bouziane F, Verstraete C, Lamberton F, Wilson CRE, Amiez C, Procyk E. Medial to lateral frontal functional connectivity mapping reveals the organization of cingulate cortex. Cereb Cortex. 2024 Aug 1;34(8):bhae322. doi: 10.1093/cercor/bhae322.

Introduction

The dynamics of cognitive processes rely both on intrinsic specificities of local neural microcircuits and on the structural properties of large-scale brain networks (Chaudhuri et al. 2015; Fontanier et al. 2022). While research has often focused on one aspect or the other, both contribute to functional dynamics. In this context we studied the organizational principles of frontal brain networks devoted to action and cognitive control.

There are multiple hypotheses on how the functional organization of frontal networks and areal specificities contribute to the neurobiological bases of cognitive control (Dixon et al. 2014). While some propose that a large-scale network encompassing fronto-parietal and latero-medial (cingulate) frontal cortical areas are recruited as a non-specific network supporting ongoing task demands, others propose a rostro-caudal anatomo-functional organization contributing to a hierarchy of cognitive-motor controls (e.g. (Badre and D'Esposito 2009; Kouneiher et al. 2009; Duncan et al. 2020). These models are not exclusive, and both assign important functional roles to the anterior cingulate and/or anterior midcingulate cortex (ACC and/or aMCC) and to its interaction with the lateral prefrontal cortex (LPFC). Several human functional brain imaging studies support a rostro-caudal functional organization of the lateral frontal cortex, but whether the cingulate cortex follows a similar principle remains unclear (Bush et al. 2000; Kouneiher et al. 2009).

Anatomically in primates, the most rostral region of the cingulate sulcus is subdivided in 2 parts: 1) the aMCC, the region extending from about the level of the anterior commissure to near the level of the rostral limit of the genu of the corpus callosum, and more anterior 2) the dorsal region of the Anterior Cingulate Cortex (ACC), the region located between the aMCC and the rostral end of the cingulate sulcus (CgS) (Vogt 2016; Amiez et al. 2019). The functional boundary between the ACC and the MCC remains unclear (Vogt 2016). Moreover, whereas the aMCC shows clear anatomo-functional homologies between humans and macaques (Amiez and Petrides 2014; Procyk et al. 2016; Amiez et al. 2019), this question is still unresolved for the ACC (Palomero-Gallagher et al. 2009; Amiez et al. 2019). The goal of the present paper is to shed new light on the functional organization of regions forming the rostral part of the CgS in the macaque brain by analyzing their connectivity with lateral frontal regions.

A primary characteristic of the aMCC is that it contains, within the CgS, the rostral Cingulate Motor Area (the so-called CMAr in macaques, and anterior Rostral Cingulate Zone -RCZa- in humans) which is somatotopically organized (i.e. it contains limb and face premotor representations) and projects weakly but directly to the spinal cord and primary motor cortices (for review see (Picard and Strick 1996; Dum and Strick 2002). Second, some neurons in the most rostral part of the CgS project to the dorsolateral prefrontal cortex (Borra et al. 2017). These anatomical specificities, including connectivity with the frontal lobe, potentially confer to the aMCC a role in interfacing motor and cognitive controls (Paus 2001). Yet, the precise extent of CMAr across animals, its somatotopic organization, its precise interplay with the dorsolateral prefrontal cortex, and how it segregates from ACC remain to be elucidated.

Previous parcellations of the cingulate region in humans, macaques and marmosets have used either diffusion tractography or resting-state fMRI (rs-fMRI) (Beckmann et al. 2009; Hutchison et al. 2012). Most studies provided grand average mappings that provide important information and broad views of cingulate functional contributions but that might be difficult to use at the individual level, and hence to decipher precise anatomical and functional landmarks. So, because cingulate interactions with lateral frontal appear to be particularly

relevant, we tested whether the connectivity between the two regions might enable identification of functional cingulate subdivisions even at the single subject level, hence revealing reliable principles of frontal cortex functional organization.

In the present investigation we first attempted to localize CMA subdivisions in macaque anterior regions of CgS at the single individual level. Second, we described the organization of functional connectivity (FC) between these cingulate regions and the lateral frontal cortex. We analyzed anesthetized rs-fMRI data from 15 rhesus macaques, to characterize the FC patterns of the aMCC and ACC regions with the lateral frontal cortex based on individual subject analysis allowing us to relate anatomical to functional features. Compared to previous studies we focused on the cortex lining the CgS, which has been the focus of most past recordings, and which contains CMAs. We also primarily restricted regions of interest to a finite list of frontal regions of interest considering regions with hand versus eye or face related functions, but confirmed our results using a non-supervised whole-brain analysis. Our results revealed that the CgS running anterior to the anterior commissure is composed of 3 main subregions aligned on the caudo-rostral axis: the hand motor/premotor field of CMAr, a face/eye premotor field, both putatively located in aMCC, and rostrally a subregion functionally connected to lateral prefrontal areas 46 and 10.

Materials and Methods

Subjects. Eighteen rhesus monkeys (*macaca mulatta*) were assessed in this study: 13 females (5-19 years old) and 5 males (10-17 years old) weighing from 5 to 13 kg. Three (2 females and 1 male, 11-12 years old) were excluded in the final analysis because of an unexplained lack of negative correlations in the functional connectivity data. All procedures followed the European Community Council Directive (directive 2010/63/UE) (Ministère de l'Agriculture et de la Forêt, Commission nationale de l'expérimentation animale) and were approved by the local ethical committee (Comité d'Ethique Lyonnais pour les Neurosciences Expérimentales, CELYNE, C2EA #42).

Animal preparation. Before anesthesia, monkeys were administered glycopyrrolate (Robinul: 0.06 mg/kg), an anticholinergic agent. After a 20-minute interval, anesthesia was induced with an intramuscular injection of tiletamine and zolazepam (Zoletil: 7 mg/kg). Subsequently, the animals were intubated and ventilated with oxygen-enriched air and different % Isoflurane depending on the monkeys (Table 1) throughout the entire scanning session. To minimize variability in measurements, an MRI-compatible stereotaxic frame (Kopf, CA, USA) secured the monkeys' heads in a sphinx position facing the back of the scanner. Breathing volume and frequency were adjusted based on the animals' weights. Physiological parameters, including heart rate and ventilation parameters (spO2 and CO2), were continuously monitored during the scan. Body temperature was maintained using warm air circulating blankets. Rs-fMRI data acquisitions were performed approximately 2 hours after anesthesia induction and at least 1 hour after the initial inhalation of isoflurane.

Monkey	% isoflurane	n slices	TR (s)	Spatial resolution	nb RUN
P	1%	28	1.8	1.7mm^3	5
K	1%	31	2	1.8mm^3	6
H	0.8%	31	1.9	1.7mm^3	5

O	1%	31	2	1.8mm^3	6
Po	1%	31	2	1.8mm^3	6
Y	1.2%	31	2	1.8mm^3	6
S	1%	25	1.7	1.7mm^3	5
V	0.8%	28	1.8	1.7mm^3	5
D	0.8%	28	1.8	1.7mm^3	5
A	1%	31	2.108	1.8mm^3	6
Ce	1.5%	31	2.108	1.8mm^3	6
Ci	1%	31	2.108	1.8mm^3	6
E	1%	31	2.108	1.8mm^3	6
Ge	1%	31	2.108	1.8mm^3	6
Gu	1%	31	2.108	1.8mm^3	6

Table 1. fMRI acquisition and anesthesia parameters for each monkey.

rs-fRMI data acquisition.
rs-fMRI data were acquired in anesthetized monkeys from a 3T Siemens Magnetom Prisma MRI scanner (Siemens Healthcare, Erlangen, Germany). Three Siemens loop coils were used: two L11 ring coils on each side of the monkey's head and one L7 above the monkey's head. A high-resolution T1-weighted anatomical scan (MPRAGE, 0.5mm^3 isotropic voxels, 144 slices, TR=3000ms, TE=366ms) was acquired for each of the 18 monkeys. rs-fMRI images covering the entire brain were obtained using a T2*-weighted gradient echo planar imaging (EPI) sequence. The acquisition parameters varied slightly for different groups of monkeys (Table 1). For each of the macaques, five or six runs of 400 volumes each were collected. Anatomical and functional data of each animal were acquired during the same session.

rs-fMRI data analysis. rs-fMRI scans were preprocessed using SPM 12.
The initial 5 volumes of each run were excluded to account for T1 equilibrium effects. Slice timing correction was performed with the time center of the volume as a reference, followed by rigid body realignment for head motion correction. Skull-stripping was executed using the bet tool from FSL software (Jenkinson et al. 2012). AFNI software (Cox 1996) was then employed for brain segmentation in both anesthetized and awake sessions on the previously skull-stripped brains. Temporal filtering extracted spontaneous slow fluctuating brain activity within the 0.01–0.1 Hz range. Linear regression removed nuisance variables, including cerebrospinal fluid and white matter signals from segmentation, as well as volumes with detected artifacts using the ART toolbox (https://www.nitrc.org/projects/artifact_detect/). The final step involved spatial smoothing with a 4-mm FWHM Gaussian kernel applied to the regression output.

Location of seeds in the prefrontal cingulate cortex.
In each hemisphere of each monkey brain, we positioned spherical 2.5mm radius seeds in the dorsal bank, fundus, and ventral bank of the CgS from the anterior commissure (i.e. caudal limit of the aMCC, see (Amiez et al. 2019) to the rostral end of the CgS (i.e. the rostral end of

the ACC, see (Amiez et al. 2019) with a spacing of 2.5mm between each seed (**Fig. 1**). The seed radius was chosen to achieve the finest-grained analysis possible, constrained by our data's spatial resolution (voxels of 1.8mm3^) and spatial smoothing (4mm). This radius has been previously validated for assessing functional connectivity in the MCC-lateral frontal and MCC-amygdala networks (Giacometti et al. 2023, 2024). Due to interindividual variability, the number of seeds differs across monkeys (see details in Table 2).

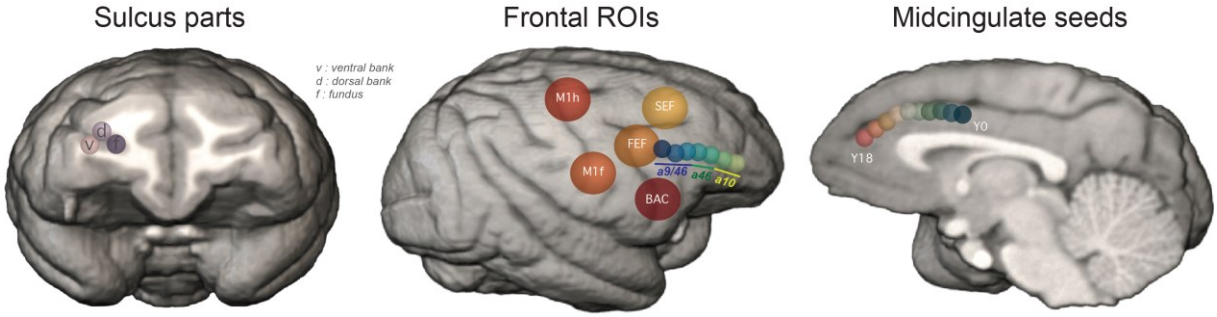

Figure 1. Position of ROIs and seeds in monkey Na in the right hemisphere. ROIs are located in the in frontal and prefrontal areas and seeds in the MCC. They are positioned in the principalis for the former and cingulate sulcus for the later and divided in three sub-regions located in the dorsal bank, the ventral bank and the fundus of their respective sulci. M1h: M1 hand, M1f: M1 face, FEF: frontal eye field, SEF: supplementary eye field, BAC: Broca's area complex.

Location of Regions of Interest (ROIs) in the lateral frontal cortex.

We first aimed to identify the hand and the face premotor representations of CMAr. We expected a stronger FC between the hand premotor representation of CMAr with the primary hand motor cortex (M1Hand). By contrast, we anticipated a stronger FC between CMAr face representation and face/oculomotor-related areas (M1Face) in the lateral frontal cortex, which includes the primary face motor cortex, the Frontal (FEF) and Supplementary (SEF) Eye Fields, and Broca's area complex (BAC). We thus positioned the following ROIs based on local sulcal morphology in each hemisphere of individual subjects (**Fig. 1**):

- M1Hand and M1Face positioned in the dorsal and the ventral part of the posterior part of the precentral gyrus respectively (He et al. 1993; Rizzolatti and Luppino 2001; Graziano et al. 2002; Giacometti et al. 2023).
- The FEF localized within the rostral bank of the genu of the arcuate sulcus (Bruce et al. 1985; Amiez and Petrides 2009).
- The SEF placed dorsally and caudally to the rostral limit of the superior part of the arcuate sulcus (Schlag and Schlag-Rey 1987).
- BAC within the fundus of the ventral part of the arcuate sulcus (Petrides et al. 2005).

Then, we aimed to examine the precise functional dialogue between the cingulate and the principal sulcus. We positioned ROIs along the entire principal sulcus, in its fundus as well as dorsal and ventral banks (**Fig. 1**). These ROIs correspond to 2.5mm radius spheres, spaced by 2.5mm. Due to interindividual variability, the number of principal sulcus ROIs differs across monkeys (see details in Table 2) All the other lateral frontal ROIs were 5mm radius spheres. We also identified morphological changes in the principal sulcus at 2 antero-posterior Y levels: the landmark 1 that corresponds to the rostral limit of the genu of the corpus callosum and the landmark 2 that corresponds to the fork at the end of the cingulate sulcus or to the rostral end if there is no fork. Interestingly, we show that these 2 landmarks delimitate anatomo-functional territories that correspond to, on the postero-anterior axis, the dorsolateral

prefrontal area 9/46, area 46, and the frontopolar area 10 (Amiez, Sallet, et al. 2023). We thus also merged the ROIs described above in each of these territories to obtain a9/46, a46, and a10 ROIs.

In the dorsolateral prefrontal cortex (dlPFC):

- Area 9/46 (a9/46) corresponds to ROIs located in the posterior part of the principal sulcus, posterior to the first morphological change in this sulcus (Landmark 1), which also appears to be at the antero-posterior Y level whereof the rostral part of the genu of the corpus callosum is observed (Amiez, Sallet, et al. 2023).
- Area 46 (a46) corresponds to ROIs located in the middle part of the principal sulcus, between Landmark 1 the level of the rostral part of the genu of the corpus callosum and the second morphological change in this sulcus (Landmark 2), which also appears to occur at the antero-posterior Y level where the rostral end of the CgS is found (Amiez, Sallet, et al. 2023).
- Area 10 (a10) corresponds to ROIs located in the rostral part of the principal sulcus, rostrally to the anteroposterior level where the rostral end of the CgS is found (Amiez, Sallet, et al. 2023).

Monkey	Seeds in CgS	ROIs in principal sulcus
P	10	7
K	11	10
H	10	7
O	10	7
Po	10	6
Y	10	7
S	10	5
V	10	5
D	10	6
A	10	7
Ce	9	6
Ci	10	5
E	10	6
Ge	10	6
Gu	10	6

Table 2. Number of seeds in Cgs and ROIs in principal sulcus for each monkey. These numbers are identical in both hemispheres.

Individual subject analyses.

For each hemisphere of each animal, Pearson correlation coefficients between the filtered BOLD signal in the seeds with the filtered BOLD signal in the ROIs were computed and normalized using the Fisher's r-to-Z transform formula. The significant threshold at the individual subject level was set to Z = 0.1 ($p < 0.05$). These normalized correlation coefficients,
which correspond to the FC strength between each seed and each ROI in individual brains, were subsequently processed with R software. Then, to assess the location in the CgS where the strongest FC is observed, we extracted the peaks of correlation (positive and negative) for each monkey and hemisphere (Fig. 2A).

Group analyses.

The following analyses were realized with R software.

ROI re-alignment

Because of the strong inter-hemispheric and inter-subject variabilities of the posterior extent of the prefrontal cortex (PFC) as marked by the genu of the arcuate sulcus on the lateral surface (Amiez, Sallet, et al. 2023), the antero-posterior Y values of the cingulate seeds were first all realigned on the antero-posterior Y values of the genu of the arcuate sulcus in each hemisphere of each individual. We chose this landmark as it was the one leading to the lowest inter-individual variance for each frontal ROI compared to the anterior commissure, the caudal and rostral limits of the genu of the corpus callosum and the fork at the rostral end of the cingulate sulcus (composed of the suprarostral sulcus ventrally and the sus-orbitalis sulcus dorsally, see Amiez et al. 2019). In addition, we spatially remapped all the seeds in the CgS according to 3 specific landmarks: 1) the anterior commissure (i.e., anteroposterior level in the caudal limit of aMCC), the genu of the arcuate sulcus, 2) the caudal (i.e., antero-posterior level of the caudal limit of the principal sulcus) and rostral genu of the corpus callosum and 3) the rostral end of the CgS (Amiez et al. 2019). To do so, we calculated the mean y axis coordinate for each landmark and scaled the seeds coordinates points to ensure consistency across all monkeys. We then performed a linear model (*model:* CgS *y coordinates ~ lateral frontal ROIs*) and extracted the r-squared value to describe the CgS FC peaks organization.

Parcellation

To test whether peaks of FC between cingulate seeds and ROIs in frontal areas were clustered in subregions of the cingulate cortex we computed a similarity matrix using the Gower distance via the 'daisy' function from the 'cluster' library (*https://cran.r-project.org/web/packages/cluster/index.html*) to capture intricate relationships between observations. We then performed a hierarchical clustering using the “Ward.D2” method. To determine the optimal number of clusters, we applied K-means models with varying values of k and computed the within-cluster sum of squares (WCSS) to identify the point where the acceleration of successive differences in WCSS was maximal. Then we assigned clusters to the data using the 'cutree' function.

The seed based parcellation described above identified that the best number of clusters in the cingulate sulcus was 3 (see results). To identify whether this parcellation stood when assessing the whole-brain FC of the cingulate sulcus, we performed a data-driven parcellation of the cingulate sulcus using a clustering algorithm on the 3D matrix of FC to classify voxels composing the gray matter of the entire brain depending on their *z* score (see Amiez et al. 2023). We expected that voxels of the cingulate sulcus mask displaying similar connectivity profiles would be clustered together revealing a sulcal subregion associated with a specific whole-brain connectivity profile. To optimize inter-subject comparisons, we reprocessed the data after registration of anatomical and functional images to the CHARM common atlas space (Seidlitz et al. 2018; Jung et al. 2021). We applied spectral clustering algorithms (Cheng et al. 2021). From the 2D matrix representing the whole-brain connectivity profile of each voxel of the cingulate sulcus mask, we computed the adjacency matrix (correlation between rows) and used the *k*-nearest neighbor to extract the similarity matrix. From the latter, the Laplacian matrix and its spectral decomposition were computed, and a *K*-means algorithm on the eigenvalues matrix provided the clusters (von Luxburg 2007). Clustering procedures were run under Python 3.8.10 using scikit-learn (Pedregosa et al.), pandas (McKinney 2010), numpy (Harris et al. 2020) and nibabel (Fanton and Thompson 2023). To select an optimal number of clusters we used silhouette index scores (ratio of the sum of between-cluster and within-cluster dispersions for all clusters (dispersion is the sum of distances squared).

Statistical analysis

To capture characteristics of the functional connectivity patterns between seeds and ROIs, we performed a general linear mixed-effect models: (*glmm: Z score ~ ROI + seed + hemisphere + interaction , with subject as random factor)* followed by post-hoc Tukey tests. To precise this pattern, we further ran one-sample student tests to calculate the difference to zero and extract the p-value on which we applied a false discovery rate correction.

Finally, to assess the proportion of negative and positive Z score value between seeds and ROIs, we first used a Wilcoxon test and then performed Dunn post-hoc tests to highlight specificities between seeds and ROIs.

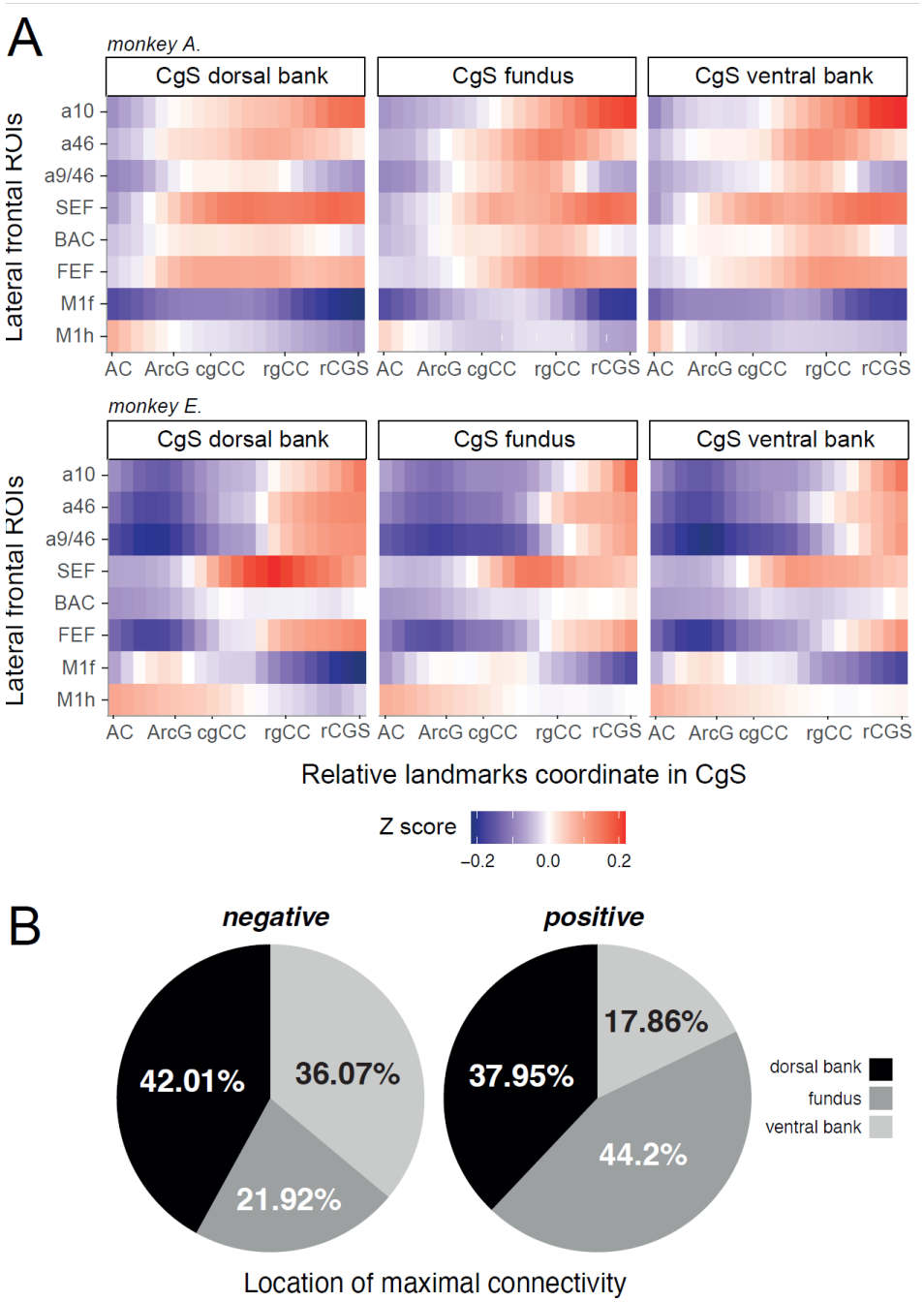

Figure 2. FC profiles between the cingulate seeds located in the dorsal bank, fundus and dorsal banks of the cingulate sulcus and lateral frontal ROIs in the left hemisphere. A. Heatmap displaying z-scores between lateral ROIs and cingulate seeds in 2 monkey subjects (top: monkey A and bottom: monkey E). In abscissa is represented the antero-posterior Y coordinate level of the cingulate seeds with the relative ant-posterior levels of key landmarks (AC = anterior commissure, ArcG = genu of the

arcuate sulcus, cgCC/rgCC = caudal/rostral limits of genu of corpus callosum, rCGS = rostral end of cingulate sulcus) and in ordinate is represented the lateral ROIs. Within the tiles, Z score correlations between both are scaled from negative (blue) to positive (red). In all examples, on the caudo-rostral axis of cingulate seeds, we observed 1) a maxima of FC with the primary hand motor ROI (M1Hand) for seeds located posterior to the genu of the arcuate sulcus (ArcG), 2) a maxima of FC with the face premotor and motor ROIs (M1Face, FEF, BAC, SEF) for seeds located 5-10 mm anterior to the genu of the arcuate sulcus, and 3) increasing FC with the dorsolateral (a9/46, a46) and the frontopolar (a10) ROIs for the seeds located rostral to the cingulate face motor area. **B**. Pie charts representing the percentages of cases where negative (left) and positive (right) peaks of FC between seeds and ROIs are located in the dorsal bank, the fundus and the ventral bank in our population (15 subjects).

Results

General FC pattern between the aMCC/ACC seeds and lateral frontal ROIs

We first sought to identify whether aMCC subregions displayed a FC pattern suggesting the presence of a somatotopy as described for cingulate motor areas (Dum and Strick 2002; Procyk et al. 2016). We thus extracted a global map of FC (as assessed by the Z values, see Materials and Methods) between the seeds located along the CgS, and the different lateral frontal cortical ROIs (**Fig. 1**). Figure 2 shows the resulting FC pattern in 2 example subjects (**Fig. 2A**), where the x-axis has been re-scaled because of the different lengths of CgS in different subjects. These examples reveal important common properties across subjects. First, at the level of the genu of the arcuate sulcus, the cingulate FC with the M1hand region presents a peak located posteriorly to those observed with other ROIs. Anterior to this region displaying increased FC with the primary hand cortex, a peak of FC is observed with the primary face area (M1Face), FEF, SEF, BAC and 9/46. Third, from this latter region to the rostral end of the CgS, the more anterior the seed is in the CgS, the stronger its FC with the SEF and the lateral dorsolateral prefrontal and frontopolar regions (a9/46, a46, a10) is. Fourth, these FC peaks are also observed in different zones of the CgS (dorsal bank, ventral bank, fundus. **Fig. 2B**), with the positive and negative FC peaks predominantly detected in the fundus/dorsal bank and the dorsal/ventral banks of the CgS respectively.

Altogether, these individual data revealed the presence of a CMA containing hand and face motor representations and showed that the cortex lying in the CgS is organized along a rostro-caudal anatomo-functional organization captured at single subject level, with more rostral (putative ACC) seeds displaying stronger FC with anterior lateral frontal ROIs than posterior (putative aMCC) seeds.

The caudo-rostral cingulate organization.

A clear spatial distribution pattern of FC peaks was observed only for positive peaks of FC with the lateral frontal ROIs in both hemispheres (left hemisphere: R2=0.42, p=0.001, right hemisphere: R2=0.45, p=0.0015) but not for negative peaks of FC (left hemisphere: R2=0.2, p=0.65, right hemisphere: R2=0.21, p=0.67). (**Fig. 3A**). This confirms at the population level that anterior-to-posterior lateral frontal ROIs are positively correlated with anterior-to-posterior parts of the CgS cortex. It also confirms the presence of a rostral hand motor representation located posterior to a face motor representation (including FC connectivity with M1face, BAC, SEF, FEF). Specifically, the hand motor representation (connected with M1hand) appears to be, at the population level, located posterior to the level of the genu of the arcuate sulcus (Y median = -2.5 / interquartile range (IQR) = 3.75 in the left and Y median = -3 / IQR = 4.25 in the right hemisphere in 18 subjects), whereas the face motor representation is located anterior to it (Y median = 6.5 / IQR = 4.75 in the left and Y median = 6 / IQR = 5 in the right hemisphere).

Interestingly, positive FC peaks were more often located in the fundus for connections with M1face, a9/46, a46 and a10 areas, and in the dorsal bank for M1 hand and FEF, BAC and SEF (**Fig. 3B**). Regarding M1face these results corroborate with previous anatomical and functional studies (Morecraft et al. 2007; Cléry et al. 2018). Negative peaks were more often located in the dorsal bank for connectivity with M1 hand, a9-46, SEF, a46 and a10, and in the ventral bank for M1face and FEF. For BAC the proportions are equal in the dorsal and ventral banks. Overall, the rostro-caudal FC organization was more pronounced for positive correlations with a significant slope (Fisher test, $p<0.01$) than for the negative ones, and the distinction between cingulate sub-regions was sharper.

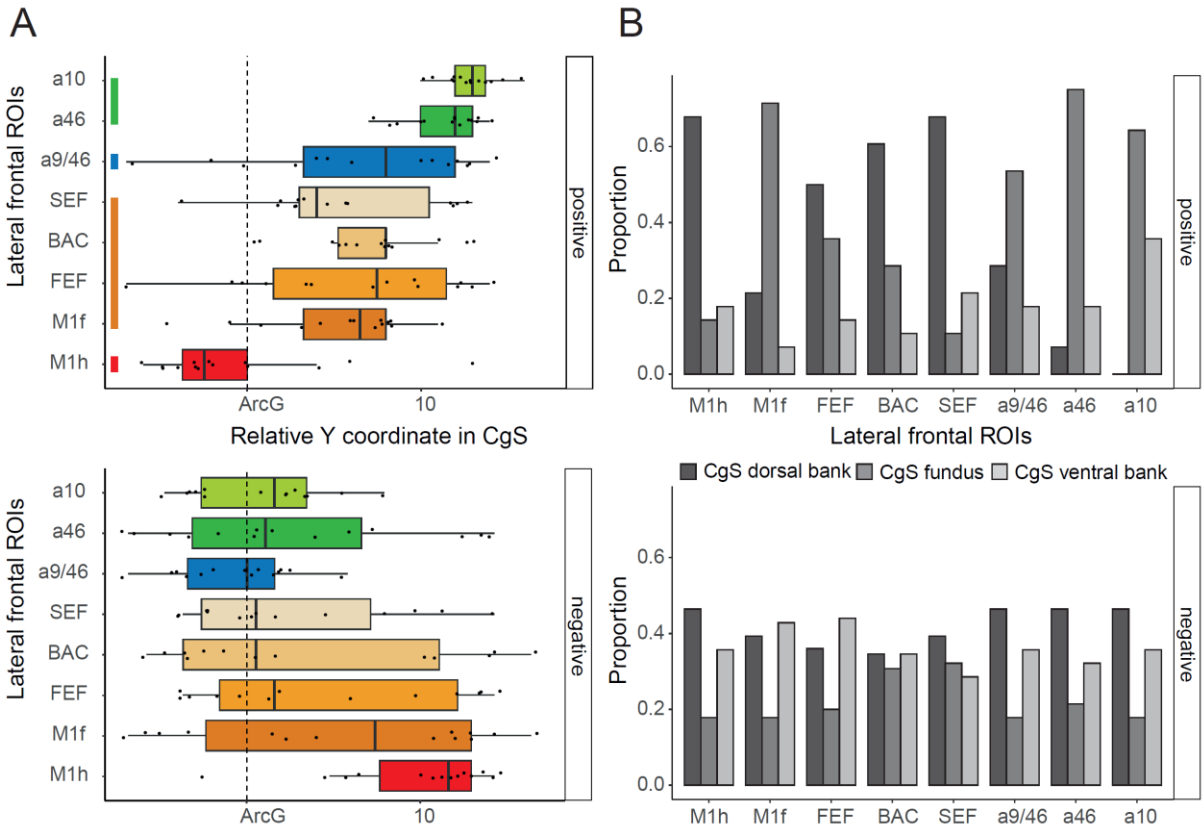

Figure 3. Rostro-caudal FC organization between the cingulate sulcal cortex and the lateral frontal ROIs. A. Antero-posterior locations of the cingulate region displaying the positive and negative FC peaks (top and bottom diagrams, respectively) with the lateral frontal ROIs in all individuals in the left hemisphere. ROIs are ordered based on their average Y coordinate. Each point represents the location of the FC peak in a given monkey. In each boxplot, the lower and upper hinges of the box correspond to the first and third quartiles respectively. Upper and lower whiskers extent from their corresponding hinges to the largest and lowest value respectively define as 1.5 x of the interquartile range. Individual data points are also represented for each boxplot. Colored lines represent the hierarchical clustering (see methods). M1h = M1 hand, M1f = M1 face. **B**. Bar plots representing the percentage of cases where the positive and negative FC peaks are located in the ventral or dorsal banks, or in the fundus of the cingulate sulcus. The 2 hemispheres are combined to have a global view of this distribution.

CMAr somatomotor representations are likely to be within the aMCC region but the position of the face field and its relationship or limit with ACC is still unresolved (Vogt 2016). Figure 3 shows that positive FC peaks related to the M1face overlap at the population level with peaks linked to FEF, SEF, BAC, and a9/46, *i.e.*, functional areas related to face, oculomotor controls, and working memory (Constantinidis and Qi 2018). The overlap thus seems to reflect the presence of a functionally specific field that we named: the face field. One hypothesis is that the limit between aMCC and ACC within the cingulate sulcus is found around the level of the genu of the corpus callosum (CC). Although the FC peak data do not show a clear limit between

the face field and a more rostral region, potentially ACC, it suggests that the rostral region displaying stronger FC with a46 and a10 is anatomically and functionally differentiated.

The dispersion of FC peaks along the CgS thus suggests partitions of the cingulate region of interest into multiple functional subdivisions. The positive FC peaks across monkeys could be clustered in 4 groups of connectivity with lateral frontal ROIs (**Fig. 3A**). Cluster 1, characterized by its FC with M1hand, is found posterior to the level of the genu of the arcuate sulcus. More anteriorly we can observe cluster 2 (M1 face, FEF, BAC, SEF), cluster 3 (a9/46) and cluster 4 (a46, a10).

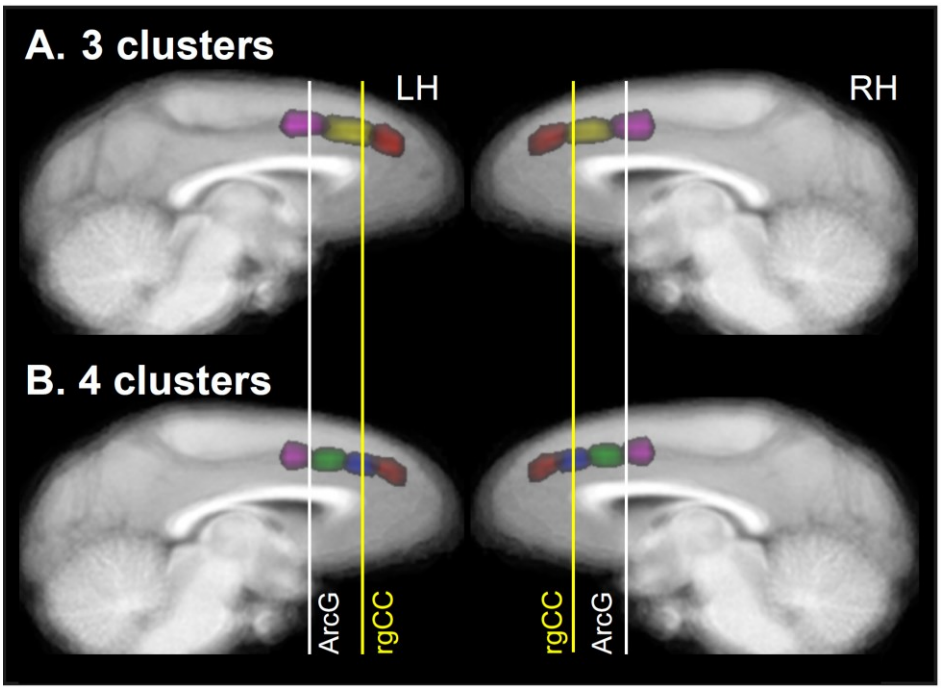

Figure 4. Whole brain data driven clustering. Clusters are defined on the group data (all monkeys). Data are displayed on the average T1 MRI volume. **A**. 3 cluster outcome. **B**. 4 cluster outcome. Note that morphological landmarks (white and yellow lines) provide indications about the relative position of clusters (as observed for each hemisphere in supplementary figure 1 and 2). White line: antero-posterior level of the genu of the arcuate sulcus. Yellow line: antero posterior level of the rostral limit of the corpus callosum.

We confirmed clustering of the cingulate region of interest with an unsupervised approach applied on each run for each hemisphere of each brain and based on the whole brain connectivity matrices. The optimal number of clusters was 3 in 62 and 68 % of cases (for left and right hemispheres respectively) cases, and 4 in 27% and 17% of cases. The reconstruction of clusters on each MRI relative to key morphological landmarks (genu of the arcuate sulcus, and anterior end of the genu of the corpus callosum) revealed a first cluster located posterior to or around the genu of the arcuate (white line in **Fig. 4A**). The most anterior cluster was anterior to the level of the genu of the corpus callosum (yellow line). Note that 3 and 4 cluster parcellations provided very coherent maps across monkeys in terms of cluster position relative to morphological landmarks (**Supplementary Fig. 1 & 2**). In the 4-parcels schema (Fig 4B, the mid subdivision is dissociated in 2 subdivisions. Note also that no clustering led to divisions of the dorsal versus ventral banks of the cingulate sulcus. Thus, the cingulate region of interest is parceled in 3 or 4 functional subregions that are found in each hemisphere at reliable positions relative to brain morphological landmarks. Remarkably the whole-brain FC analysis showed clear dissociations between the cingulate subdivisions in terms of large-scale connectivity. In the 3-parcel schema of the cingulate sulcus (Fig 5), we first observed a caudo-

rostral dissociation in which the i) posterior, ii) mid, and iii) anterior subdivision displays FC, respectively, with i) hand motor/premotor cortex (i.e. M1 Hand, PMd) and putamen, ii) face/eye motor/premotor (M1Face, BAC, FEF), caudal prefrontal cortex (a9/46, SEF), as well as putamen/caudate nucleus, and iii) anterior prefrontal cortex (a46, a10), the anterior insula, the amygdala, the caudate nucleus, the Posterior Cingulate Cortex (PCC), and the superior temporal sulcus (STS). In addition, we observed that the posterior and mid subdivisions share FC with the posterior parietal cortex (PPC), posterior insula, precuneus (PRC) and temporal cortex (TpT, and superior temporal gyrus - STG). Thus, the whole brain analysis revealed clear anatomo-functionnal dissociations between the large-scale networks centered on the different cingulate subdivisions.

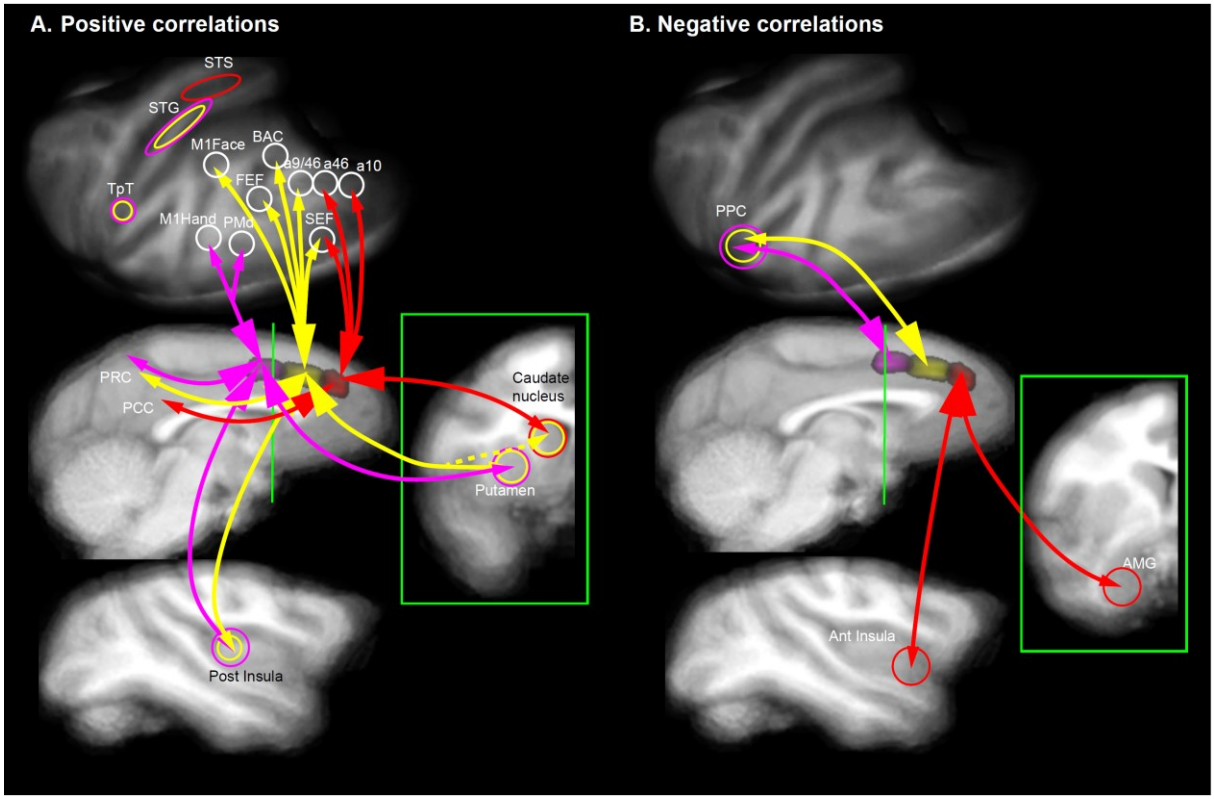

Figure 5. Whole-brain functional connectivity of the cingulate sulcus. A. Positive correlations. **B.** Negative correlations. The green line indicates the location of the coronal section in green box. STS: superior temporal sulcus, STG: superior temporal gyrus, TpT: temporo-parietal cortex, PMd: dorsal premotor area, PRC: precuneus, PCC: posterior cingulate cortex, PPC: posterior parietal cortex, AMG: amygdala., Ant and Post Insula: anterior and posterior insula.

FC organization between the cingulate and principal sulci

Recordings in monkeys but also functional brain imaging studies in humans suggest that the aMCC and subregions of the dlPFC are co-activated for cognitive control regulation (Shenhav et al. 2013; Kolling et al. 2018). Whether such co-activations relate to specific anatomo-functional organizations is thus a central question. We assessed the fine-grained organization of the FC between seeds located in the various subdivisions and along the CgS and the ROIs located along the principal sulcus (*in* dorsal and ventral banks and fundus subdivisions). The analyses provided 2D maps of FC between these different subdivisions (**Fig. 6**).

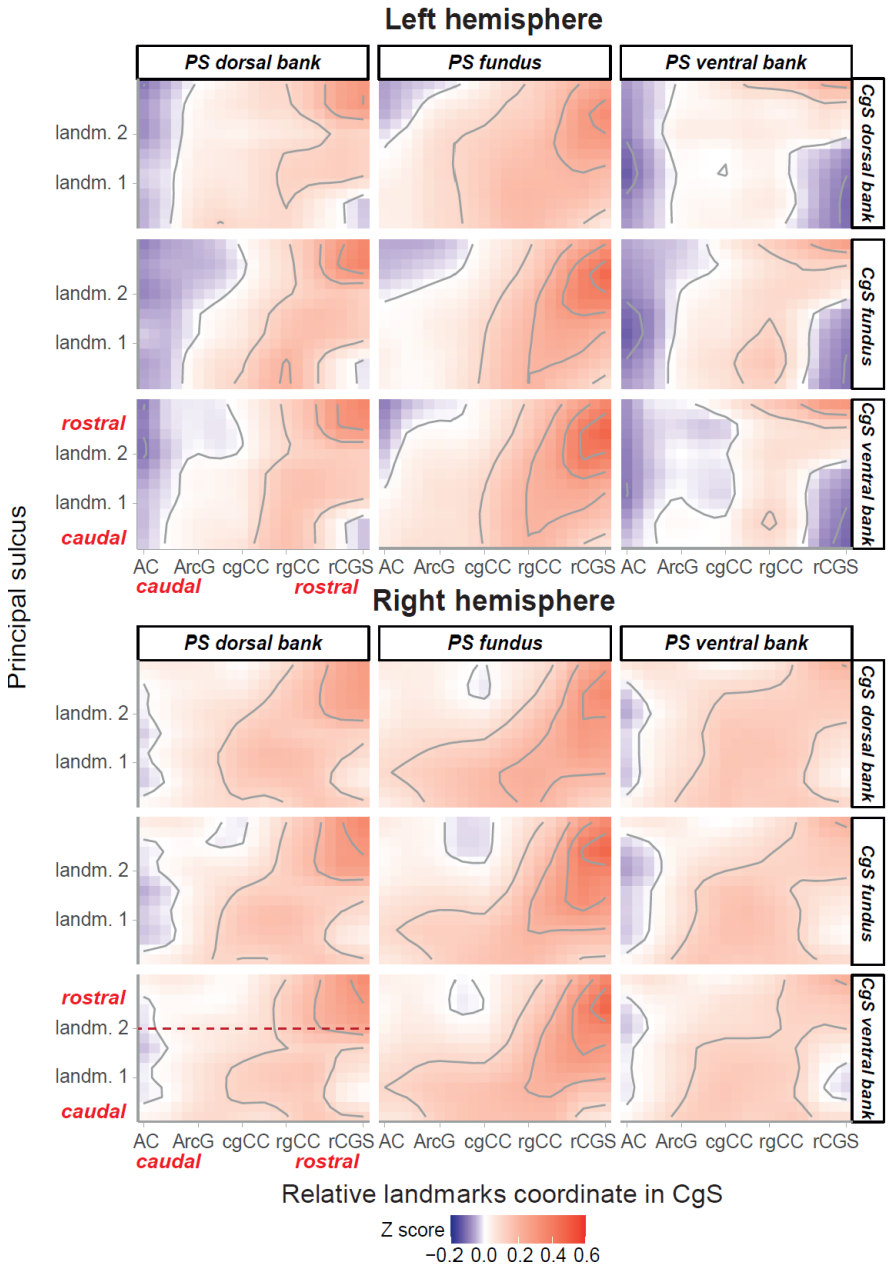

Figure 6. Rostro-caudal organization of the FC between the ventral bank, fundus et dorsal bank of the principal and the cingulate sulci in the left and right hemispheres across the population. Correlation map of the FC between principalis sulcus and cingulate sulcus, represented by the Z-value (red to blue gradient for positive to negative correlations respectively). Data are realigned on specific landmarks for each monkey. AC = anterior commissure, ArcG = genu of the arcuate sulcus, cgCC/rgCC = caudal/rostral limits of genu of corpus callosum, rCGS = rostral end of cingulate sulcus.

The pattern of FC followed a rostro-caudal organization with stronger positive correlations between the BOLD signals in the rostral part of the CgS and the anterior most part of the principal sulcus (**Fig. 6**). The increased FC involved more reliably the dorsal bank and the fundus, and less the ventral bank, of the sulcus principalis located anterior to landmark 2 in both hemispheres (*i.e.,* anterior to the level of the rostral end of the CgS. See Materiel and Methods, *student test, p<0.001.* **Supplementary Fig.3**). This is of great interest because previous studies have shown that morphological landmarks within the principal sulcus could be landmarks of cytoarchitectonic areas, landmark 2 noted here being related to the transition between area 46 and area 10 (Amiez, Sallet, et al. 2023). Note, however, that the FC pattern between the cingulate and the principal sulci differed significantly between the 2 hemispheres

(*see model in methods, Main effect of Principal-Sulcus_ROI: p<2.2e-16, Main effect of Cingulate-Sulcus_SEED: p<2.2e-16; Main effect of Hemisphere: p<2.2e-16*). The FC pattern varied also according to the sulcus subdivisions - dorsal, ventral and fundus. In the left hemisphere, the patterns of FC differed between all cingulate parts (*Tukey multiple comparisons test: p<0.0001*) and all principal sulcus parts (*Tukey multiple comparisons test: p<0.0001*). In the right hemisphere, the FC patterns differed when comparing data for the dorsal bank and the fundus of the principal sulcus (*Tukey multiple comparisons test: p<0.002*). From the point of view of the CgS, the FC patterns differed between the dorsal and the ventral banks (*Tukey multiple comparisons test: p<0.04*) and between the fundus and ventral bank (*Tukey multiple comparisons test: p<0.004*). Supplementary figure 3 shows at what level, and for which sulci parts, the cingulate-principalis connectivity differed from 0. It shows that the FC between Cgs and PS was more pronounced between the fundus parts in both hemispheres.

Finally, negative correlations were more pronounced in the left hemisphere than in the right hemisphere (*Wilcoxon test, p<0.005*) and more specifically in the ventral bank of the principal sulcus (*Dunn tests, p<0.00001*).

Discussion

The present study revealed that cingulo-lateral frontal cortical networks in the macaque brain are organized along a caudo-rostral axis. Using precise and reliable anatomical landmarks, we described a fine-grained anatomo-functional organization. Specifically, in the caudal most CgS seeds, we identified across individual subjects that the hand-related premotor representations of CMAr were located more often in the dorsal bank of the CgS and caudal to the level of the genu of the arcuate sulcus, whereas the face-related representation were located more often in the fundus of the CgS and rostral to the genu of the arcuate. In addition, more rostral parts of the CgS were more strongly functionally connected with more rostral parts of the principal sulcus. Overall, the study revealed a tripartition of the CgS in the frontal lobe shedding new light on the organization of the cingulo-lateral frontal network in non-human primates (**Fig. 5**).

Our results also revealed the presence of a rostro-caudal FC organization between the CgS and the principal sulcus. Although this organization involves the dorsal/ventral banks and fundus of sulci, it appears stronger when considering the fundus of the principal sulcus in both hemispheres (**Fig. 3**). These results fit with the known tract-tracing data between these two regions (Barbas and Pandya 1989; Joyce et al. 2020). By contrast, the most caudal part of the CgS studied here, that includes a CMAr hand motor representation, appears mostly negatively correlated with the principal sulcus, thus reinforcing the existence of anticorrelated networks, here between a motor and a cognitive network.

Somatotopy in CMAr and cingulate functional organization

The respective locations of CMAr hand- and face-related fields in the CgS, detected with FC peaks with M1, are consistent with the literature. Anatomical and functional studies showed that these fields are respectively located in the dorsal bank and fundus of the CgS, with the face-related field located rostral to the hand-related one (**Fig. 2**) (Dum and Strick 2002; Morecraft et al. 2007; Procyk et al. 2016; Cléry et al. 2018). The hand-related subdivision (as represented by FC peaks, **Fig. 2**) was located in the CgS between the level of the anterior commissure and the level of the genu of the arcuate sulcus (ArcG). The core of the face-related

representation was located on average 6mm anterior to the level of ArcG. The known cytoarchitectonic organization suggests that both the hand and face fields of CMAr belong to the aMCC region (Vogt 2005; Amiez et al. 2019). The caudal and rostral limits of aMCC are presumably at the level of, respectively, the anterior commissure and the rostral limit of the genu of the corpus callosum (rgCC) (Vogt et al. 2003; Vogt et al. 2006; Palomero-Gallagher et al. 2009; Amiez et al. 2019).

The data suggest that more caudal versus rostral cingulate seeds displayed positive FC with respectively more caudal versus rostral frontal ROIs (**Fig. 2**). This aligns with previous studies in human and non-human primates (Loh et al. 2018; Giacometti et al. 2022). However, our study reveals a more intricate relationship. Indeed, our clustering suggests that the CgS part under study is subdivided in 3 or in some cases 4 functional sectors: a caudal sector involved with hand-related motor and premotor regions, a middle sector displaying functional connectivity with frontal areas involved with oral and oculomotor/attentional functions (M1face, BAC, FEF, SEF, a9/46), and a more rostral sector connected to anterior prefrontal areas (a46 and a10). The middle face field sector supposedly corresponds to the region the most recorded in neurophysiological studies displaying neural activity related to outcome processing, behavioral shifting, and exploratory decisions (Procyk et al. 2016). This region might even be subdivided in two parts, one related to the oral domain and one to the oculomotor domain. This additional subdivision would further explain why 4 cluster subdivisions was observed in more than 15% of cases among our monkey population. However, the limited spatial resolution of our fMRI data prevents us from clarifying any further. The rostral limit of the face field sector within the CgS is located at the rostro-caudal level of the genu of the corpus callosum. This might represent the limit between aMCC and ACC in the cingulate sulcus, which is also suggested by the clustering method. The whole-brain FC is also showing a shift in large scale connectivity between the 2 posterior and the most anterior cingulate subregion, the anterior part of the CgS being more functionally connected with limbic regions (amygdala and anterior insula) and anterior lateral prefrontal regions (a46, a10) (**Fig. 5**). However, a definitive description of this aMCC-ACC limit will require a devoted cytoarchitectonic and connectivity analysis.

Importantly, the parcellation results, whether the whole-brain data-driven parcellation or the unsupervised clustering within our network of interest, fit perfectly with previous analyses in macaques showing 3 sectors in the cingulate cortex associated with somato-motor (CMAr hand), attention-orienting (face/eye) and executive networks (Hutchison et al. 2012). The network embedding the attention-orienting sector delineated by Hutchison and colleagues overlaps with a similar frontal anatomical network encompassing regions involved with oral/face motor control and proposed to play a role in communication/emotions and reward processing (Ferrari et al. 2017). We proposed that the mere existence of a CMAr face-related network involved in information-/reward- seeking, shifting and decision making reflects a principle by which such functions are embodied, i.e. that their root mechanisms, and potentially computational principle, are intimately related to effector specificities, the functions being ecologically bounded to these effectors (Procyk et al. 2016).

Parcellations of the cingulate cortex in humans based on connectivity have shown multiple clusters that, for the most anterior ones at least, fit with our observations in macaques in terms of rostro-caudal organization (Beckmann et al. 2009). Beckman and colleagues, using diffusion tractography, found that a caudal cingulate cluster had major premotor connectivity while a more rostral cluster had more prefrontal connectivity. Comparative functional network analyses between humans and macaques have shown good homologies between

cingulate subdivisions (Neubert et al. 2015). Interestingly, functional connectivity clustering of the homolog cingulate region in marmosets led to a clear separation at the level of the genu of the corpus callosum, the more caudal cluster being connected to premotor regions, and the anterior ones to prefrontal regions (Schaeffer et al. 2018). Finally, human and marmoset cingulate parcellations showed important similarity regarding their functional connectivity with lateral frontal regions (Schaeffer et al. 2020). Human, macaque and marmoset have thus very conserved subdivisions of the cingulate region although no direct comparisons have been done between the three species.

Brain morphology landmarks and functional connectivity

Cingulate subregions were consistently observed in particular locations relative to morphological landmarks. This converges with a growing body of evidence suggesting tight relationships between gross morphology, sulcal organization, cytoarchitectonic organization, functional organization, and behavior in macaques (Morecraft et al. 2007; García-Cabezas and Barbas 2014; Procyk et al. 2016; Cléry et al. 2018), chimpanzees (Keller et al. 2009; Amiez et al. 2021), in humans (Vogt et al. 1995; White 1997; Amiez et al. 2006; Amiez and Petrides 2007; Amiez et al. 2013; Loh et al. 2018; Lopez-Persem et al. 2019; Loh et al. 2020) and even in primate comparatives studies (Amiez et al. 2019; Amiez, Sallet, et al. 2023; Amiez, Verstraete, et al. 2023). Such relationships are to be expected given that the cytoarchitectonic organization might constrain the connectivity of a given area (Passingham et al. 2002) and that the protomap tightly links sulcal pits with cytoarchitectonic organization (Rakic 1988; Régis et al. 2005; Fischl et al. 2008), see also (Amiez, Sallet, et al. 2023) for more details about the possible foundations of such relationships). Anatomo-functional maps and morphological landmarks may thus serve as additional indices to locate specific functional subregions. This would be particularly relevant for targeted approaches such as anatomical tracer injections, electrophysiological recordings, or transcranial ultrasound stimulation. Complemented with human-macaque comparative studies of frontal sulcal organizations, these maps could be transposed to humans.

From a clinical point of view, prefrontal to cingulate networks are proposed to play a role in the etiology and manifestations of various neurological and psychiatric disorders. Dysfunctional connectivity between these regions have been observed in a range of conditions including attention deficit hyperactivity disorder (Bush et al. 2005), obsessive-compulsive disorder (Menzies et al. 2008), schizophrenia (Fornito et al. 2009), and mood disorders (Phillips et al. 2003). Thus, characterizing the precise functional connectivity patterns between cingulate and lateral frontal areas could provide markers to quantify pathological connectivity as well as to define targets for potential focused treatments.

Dorso-ventral heterogeneity in the principal sulcus

In our study, we focused on the functional connectivity and data-driven parcellation of the principal sulcus, which revealed a clear rostro-caudal segmentation into three distinct regions. However, we acknowledge the existing evidence for dorsoventral heterogeneity in this area, as detailed by Barbas and Pandya (1989), Morecraft et al. (2015), and Rapan et al. (2023). These studies underscore cytoarchitectonic differences between the dorsal and ventral banks of the principal sulcus, which our approach did not detect. There are several reasons for this discrepancy. First, our whole-brain functional connectivity analysis might lack the sensitivity to detect subtle dorsoventral differences. Such differences could be specific to particular

networks and not broadly reflected across the entire brain, making them challenging to identify with the broad scope of our analysis. Second, the limitations of rsfMRI may also play a role. While rsfMRI is a powerful tool for mapping functional connectivity, its spatial resolution might not be fine enough to capture the detailed cytoarchitectonic distinctions between the dorsal and ventral banks of the principal sulcus. These subtle differences likely require more precise imaging techniques or targeted, high-resolution analyses beyond the capabilities of conventional rsfMRI. Furthermore, a comprehensive cytoarchitectonic study that maps the precise boundaries between Areas 10, 46, and 9/46 along the entire extent of the principal sulcus is essential for future research. Such a study would provide a definitive anatomical framework to complement and refine our functional connectivity findings, ensuring that both the functional and structural nuances of this region are thoroughly understood.

Negative functional connectivity

Interestingly, a marginal (non-significant) reverse rostro-caudal organization was captured by the distribution of negative FC peaks (more caudal cingulate seeds display a negative FC peak with more rostral frontal ROIs; **Fig. 2**). For example, the FC between the CgS and M1hand is characterized by a positive FC peak located in the posterior part of aMCC and a negative FC peak in the ACC (**Fig 2**). The interpretation and relevance of negative correlations in BOLD signal in general is still misunderstood and disputed (Biswal et al. 1995; Chang and Glover 2009; Giove et al. 2009; Murphy et al. 2009; Weissenbacher et al. 2009) and often neglected (Chen and Calhoun 2011). However, recent hypotheses suggest that two anticorrelated systems such as the Default Mode Network (DMN, involved in some introspection activity at rest, see (Gusnard et al. 2001; Raichle et al. 2001) and the Dorsal Attentional Network (DAN, involved in the performance of cognitive tasks, are competitive networks that cannot act at the same time and are thus "inhibiting" each other depending on the context (Fransson 2005; Kelly et al. 2008; Chai et al. 2012; Chai et al. 2014). Such a process appears critical to obtain a dynamic but stable system (Saberi et al. 2021), its disruption being observed in numerous neurological and psychiatric disorders (Wang and Fan 2007; Sun et al. 2012; Patriat et al. 2016; Posner et al. 2016; Whitfield-Gabrieli et al. 2018). Anterior versus posterior subdivisions of the cingulate region devoted to respectively emotional and cognitive processing have been proposed in humans, with a putative reciprocal suppression (Bush et al. 2000). Based on this literature, our results might suggest that the recruitment of CMAr, which is located in the aMCC, is associated with the deactivation of ACC regions, or rather that regions involved with motor control (through links with the primary motor cortex) are naturally in opposition with regions involved with the lateral prefrontal regions. Note however that our data were obtained from anesthetized states (see Limitations).

Limitation

Our results were fairly reliable across our 15 monkeys despite the fact that they were acquired under isoflurane anesthesia, which is known to affect FC (Hutchison et al. 2014; Barttfeld et al. 2015; Lv et al. 2016) In particular, anesthesia reduces FC strength in general and reduces negative correlations (at least in frontal networks) (Hori et al. 2020; Giacometti et al. 2022). We have also shown that it prevents the assessment of posterior cingulate motor areas (CMAc) as they are strongly connected with the primary motor areas (as opposed to CMAr) and these latter regions are shut down by anesthesia (Giacometti et al. 2022). However, we excluded here the assessment of the FC of CMAc. Thus, although anesthesia decreases

globally the FC strength in our network of interest, it does not change its overall pattern (Giacometti et al. 2022). Furthermore, it allowed us to perform our subject-by-subject analysis in a larger dataset (18 monkeys), and importantly our results demonstrated the reliability of the use of sulcal individual morphological patterns to extract fine-grained FC patterns in the frontal cortex.

Conclusion

The present study revealed that the cingulate organization can be captured in individual monkey brains based on the functional connectivity pattern of the CgS and the lateral frontal cortex. We identified the fine-grained FC interplay between the cingulate and the principal sulci that might sustain the functional dialogue between these regions. Importantly, this organization can also be predicted from local morphological features that all individuals possess, thus providing a framework usable with short resting-state MRI scans to precisely target cingulate or lateral frontal cortical regions. Finally, subdivisions of the cingulate region of interest are characterized by their embedding in dissociated functional networks, whose specificity should be considered in order to understand the computational bases of cingulate functions.

Authors' contributions

E.P. and C.A. organized the project. F.L. defined and optimized neuroimaging acquisition protocols. C.G., D.A-C., A.D., C.W., M.Di., and F.H.-B. acquired neuroimaging data. C.V. did the clusterisation algorithm. M.Du., E.P., and C.A. analyzed and interpreted data. M.Du., E.P., C.A. and C.W. wrote the article. The authors thank V Vezoli, N. Ferroukhi, and C Nay for administrative help and support, and A. Bellemin-Menard, F. Da Silva Couto, J Lachaud, G Gardechaux, and M Filiptchenko for help and support with animal welfare and care.

Funding

This work was supported by Fondation pour la Recherche Médicale, by the ANR-19-CE37-0008-01, ANR-18-CE37-0016 and ANR-18-CE37-0012, and was performed within the framework of the LABEX CORTEX (ANR-11-LABX-0042) of Université de Lyon operated by the French National Research Agency (ANR). E.P. and C.A. are employed by the Centre National de la Recherche Scientifique.

References

Amiez C, Joseph JP, Procyk E. 2006. Reward Encoding in the Monkey Anterior Cingulate Cortex. Cerebral Cortex. 16(7):1040–1055. doi:10.1093/cercor/bhj046.

Amiez C, Neveu R, Warrot D, Petrides M, Knoblauch K, Procyk E. 2013. The Location of Feedback-Related Activity in the Midcingulate Cortex Is Predicted by Local Morphology. J Neurosci. 33(5):2217–2228. doi:10.1523/JNEUROSCI.2779-12.2013.

Amiez C, Petrides M. 2007. Selective involvement of the mid-dorsolateral prefrontal cortex in the coding of the serial order of visual stimuli in working memory. Proc Natl Acad Sci USA. 104(34):13786–13791. doi:10.1073/pnas.0706220104.

Amiez C, Petrides M. 2009. Anatomical organization of the eye fields in the human and non-human primate frontal cortex. Progress in Neurobiology. 89(2):220–230. doi:10.1016/j.pneurobio.2009.07.010.

Amiez C, Petrides M. 2014. Neuroimaging Evidence of the Anatomo-Functional Organization of the Human Cingulate Motor Areas. Cerebral Cortex. 24(3):563–578. doi:10.1093/cercor/bhs329.

Amiez C, Sallet J, Giacometti C, Verstraete C, Gandaux C, Morel-Latour V, Meguerditchian A, Hadj-Bouziane F, Ben Hamed S, Hopkins WD, et al. 2023. A revised perspective on the evolution of the lateral frontal cortex in primates. Sci Adv. 9(20):eadf9445. doi:10.1126/sciadv.adf9445.

Amiez C, Sallet J, Hopkins WD, Meguerditchian A, Hadj-Bouziane F, Ben Hamed S, Wilson CRE, Procyk E, Petrides M. 2019. Sulcal organization in the medial frontal cortex provides insights into primate brain evolution. Nat Commun. 10(1):3437. doi:10.1038/s41467-019-11347-x.

Amiez C, Sallet J, Novek J, Hadj-Bouziane F, Giacometti C, Andersson J, Hopkins WD, Petrides M. 2021. Chimpanzee histology and functional brain imaging show that the paracingulate sulcus is not human-specific. Commun Biol. 4(1):54. doi:10.1038/s42003-020-01571-3.

Amiez C, Verstraete C, Sallet J, Hadj-Bouziane F, Ben Hamed S, Meguerditchian A, Procyk E, Wilson CRE, Petrides M, Sherwood CC, et al. 2023. The relevance of the unique anatomy of the human prefrontal operculum to the emergence of speech. Commun Biol. 6(1):693. doi:10.1038/s42003-023-05066-9.

Badre D, D'Esposito M. 2009. Is the rostro-caudal axis of the frontal lobe hierarchical? Nat Rev Neurosci. 10(9):659–669. doi:10.1038/nrn2667.

Barbas H, Pandya DN. 1989. Architecture and intrinsic connections of the prefrontal cortex in the rhesus monkey. J of Comparative Neurology. 286(3):353–375. doi:10.1002/cne.902860306.

Barttfeld P, Uhrig L, Sitt JD, Sigman M, Jarraya B, Dehaene S. 2015. Signature of consciousness in the dynamics of resting-state brain activity. Proc Natl Acad Sci USA. 112(3):887–892. doi:10.1073/pnas.1418031112.

Beckmann M, Johansen-Berg H, Rushworth MFS. 2009. Connectivity-Based Parcellation of Human Cingulate Cortex and Its Relation to Functional Specialization. J Neurosci. 29(4):1175–1190. doi:10.1523/JNEUROSCI.3328-08.2009.

Biswal B, Zerrin Yetkin F, Haughton VM, Hyde JS. 1995. Functional connectivity in the motor cortex of resting human brain using echo-planar mri. Magnetic Resonance in Med. 34(4):537–541. doi:10.1002/mrm.1910340409.

Borra E, Ferroni CG, Gerbella M, Giorgetti V, Mangiaracina C, Rozzi S, Luppino G. 2017. Rostro-caudal Connectional Heterogeneity of the Dorsal Part of the Macaque Prefrontal Area 46. Cerebral Cortex. 29(2):485–504. doi:10.1093/cercor/bhx332.

Bruce CJ, Goldberg ME, Bushnell MC, Stanton GB. 1985. Primate frontal eye fields. II. Physiological and anatomical correlates of electrically evoked eye movements. Journal of Neurophysiology. 54(3):714–734. doi:10.1152/jn.1985.54.3.714.

Bush G, Luu P, Posner MI. 2000. Cognitive and emotional influences in anterior cingulate cortex. Trends in Cognitive Sciences. 4(6):215–222. doi:10.1016/S1364-6613(00)01483-2.

Bush G, Valera EM, Seidman LJ. 2005. Functional Neuroimaging of Attention-Deficit/Hyperactivity Disorder: A Review and Suggested Future Directions. Biological Psychiatry. 57(11):1273–1284. doi:10.1016/j.biopsych.2005.01.034.

Chai XJ, Castañón AN, Öngür D, Whitfield-Gabrieli S. 2012. Anticorrelations in resting state networks without global signal regression. NeuroImage. 59(2):1420–1428. doi:10.1016/j.neuroimage.2011.08.048.

Chai XJ, Ofen N, Gabrieli JDE, Whitfield-Gabrieli S. 2014. Selective Development of Anticorrelated Networks in the Intrinsic Functional Organization of the Human Brain. Journal of Cognitive Neuroscience. 26(3):501–513. doi:10.1162/jocn_a_00517.

Chang C, Glover GH. 2009. Relationship between respiration, end-tidal CO2, and BOLD signals in resting-state fMRI. NeuroImage. 47(4):1381–1393. doi:10.1016/j.neuroimage.2009.04.048.

Chaudhuri R, Knoblauch K, Gariel M-A, Kennedy H, Wang X-J. 2015. A Large-Scale Circuit Mechanism for Hierarchical Dynamical Processing in the Primate Cortex. Neuron. 88(2):419–431. doi:10.1016/j.neuron.2015.09.008.

Chen Z, Calhoun VD. 2011. Two pitfalls of BOLD fMRI magnitude-based neuroimage analysis: Non-negativity and edge effect. Journal of Neuroscience Methods. 199(2):363–369. doi:10.1016/j.jneumeth.2011.05.018.

Cheng L, Zhang Y, Li G, Wang J, Sherwood C, Gong G, Fan L, Jiang T. 2021. Connectional asymmetry of the inferior parietal lobule shapes hemispheric specialization in humans, chimpanzees, and rhesus macaques. eLife. 10:e67600. doi:10.7554/eLife.67600.

Cléry J, Amiez C, Guipponi O, Wardak C, Procyk E, Ben Hamed S. 2018. Reward activations and face fields in monkey cingulate motor areas. Journal of Neurophysiology. 119(3):1037–1044. doi:10.1152/jn.00749.2017.

Constantinidis C, Qi X-L. 2018. Representation of Spatial and Feature Information in the Monkey Dorsal and Ventral Prefrontal Cortex. Front Integr Neurosci. 12:31. doi:10.3389/fnint.2018.00031.

Cox RW. 1996. AFNI: Software for Analysis and Visualization of Functional Magnetic Resonance Neuroimages. Computers and Biomedical Research. 29(3):162–173. doi:10.1006/cbmr.1996.0014.

Dixon ML, Fox KCR, Christoff K. 2014. Evidence for rostro-caudal functional organization in multiple brain areas

related to goal-directed behavior. Brain Research. 1572:26–39. doi:10.1016/j.brainres.2014.05.012.
Dum R, Strick P. 2002. Motor areas in the frontal lobe of the primate. Physiology & Behavior. 77(4–5):677–682. doi:10.1016/S0031-9384(02)00929-0.
Duncan J, Assem M, Shashidhara S. 2020. Integrated Intelligence from Distributed Brain Activity. Trends in Cognitive Sciences. 24(10):838–852. doi:10.1016/j.tics.2020.06.012.
Fanton S, Thompson WH. 2023. *NetPlotBrain* : A Python package for visualizing networks and brains. Network Neuroscience. 7(2):461–477. doi:10.1162/netn_a_00313.
Ferrari PF, Gerbella M, Coudé G, Rozzi S. 2017. Two different mirror neuron networks: The sensorimotor (hand) and limbic (face) pathways. Neuroscience. 358:300–315. doi:10.1016/j.neuroscience.2017.06.052.
Fischl B, Rajendran N, Busa E, Augustinack J, Hinds O, Yeo BTT, Mohlberg H, Amunts K, Zilles K. 2008. Cortical Folding Patterns and Predicting Cytoarchitecture. Cerebral Cortex. 18(8):1973–1980. doi:10.1093/cercor/bhm225.
Fontanier V, Sarazin M, Stoll FM, Delord B, Procyk E. 2022. Inhibitory control of frontal metastability sets the temporal signature of cognition. eLife. 11:e63795. doi:10.7554/eLife.63795.
Fornito A, Yücel M, Patti J, Wood SJ, Pantelis C. 2009. Mapping grey matter reductions in schizophrenia: An anatomical likelihood estimation analysis of voxel-based morphometry studies. Schizophrenia Research. 108(1–3):104–113. doi:10.1016/j.schres.2008.12.011.
Fransson P. 2005. Spontaneous low-frequency BOLD signal fluctuations: An fMRI investigation of the resting-state default mode of brain function hypothesis. Human Brain Mapping. 26(1):15–29. doi:10.1002/hbm.20113.
García-Cabezas MÁ, Barbas H. 2014. A direct anterior cingulate pathway to the primate primary olfactory cortex may control attention to olfaction. Brain Struct Funct. 219(5):1735–1754. doi:10.1007/s00429-013-0598-3.
Giacometti C, Amiez C, Hadj-Bouziane F. 2023. Multiple routes of communication within the amygdala-mPFC network: A comparative approach in humans and macaques. Current Research in Neurobiology. 5:100103. doi:10.1016/j.crneur.2023.100103.
Giacometti C, Dureux A, Autran-Clavagnier D, Wilson CRE, Sallet J, Dirheimer M, Procyk E, Hadj-Bouziane F, Amiez C. 2022. Frontal cortical functional connectivity is impacted by anaesthesia in macaques. Cerebral Cortex. 32(18):4050–4067. doi:10.1093/cercor/bhab465.
Giove F, Gili T, Iacovella V, Macaluso E, Maraviglia B. 2009. Images-based suppression of unwanted global signals in resting-state functional connectivity studies. Magnetic Resonance Imaging. 27(8):1058–1064. doi:10.1016/j.mri.2009.06.004.
Graziano MSA, Taylor CSR, Moore T. 2002. Complex Movements Evoked by Microstimulation of Precentral Cortex.
Gusnard DA, Akbudak E, Shulman GL, Raichle ME. 2001. Medial prefrontal cortex and self-referential mental activity: Relation to a default mode of brain function. Proc Natl Acad Sci USA. 98(7):4259–4264. doi:10.1073/pnas.071043098.
Harris CR, Millman KJ, Van Der Walt SJ, Gommers R, Virtanen P, Cournapeau D, Wieser E, Taylor J, Berg S, Smith NJ, et al. 2020. Array programming with NumPy. Nature. 585(7825):357–362. doi:10.1038/s41586-020-2649-2.
He S, Dum R, Strick P. 1993. Topographic organization of corticospinal projections from the frontal lobe: motor areas on the lateral surface of the hemisphere. J Neurosci. 13(3):952–980. doi:10.1523/JNEUROSCI.13-03-00952.1993.
Hori Y, Schaeffer DJ, Gilbert KM, Hayrynen LK, Cléry JC, Gati JS, Menon RS, Everling S. 2020. Altered Resting-State Functional Connectivity Between Awake and Isoflurane Anesthetized Marmosets. Cerebral Cortex. 30(11):5943–5959. doi:10.1093/cercor/bhaa168.
Hutchison RM, Hutchison M, Manning KY, Menon RS, Everling S. 2014. Isoflurane induces dose-dependent alterations in the cortical connectivity profiles and dynamic properties of the brain's functional architecture: Dose-Dependent Isoflurane Effects. Hum Brain Mapp. 35(12):5754–5775. doi:10.1002/hbm.22583.
Hutchison RM, Womelsdorf T, Gati JS, Leung LS, Menon RS, Everling S. 2012. Resting-State Connectivity Identifies Distinct Functional Networks in Macaque Cingulate Cortex. Cerebral Cortex. 22(6):1294–1308. doi:10.1093/cercor/bhr181.
Jenkinson M, Beckmann CF, Behrens TEJ, Woolrich MW, Smith SM. 2012. FSL. NeuroImage. 62(2):782–790. doi:10.1016/j.neuroimage.2011.09.015.
Joyce MKP, García-Cabezas MÁ, John YJ, Barbas H. 2020. Serial Prefrontal Pathways Are Positioned to Balance Cognition and Emotion in Primates. J Neurosci. 40(43):8306–8328. doi:10.1523/JNEUROSCI.0860-20.2020.
Jung B, Taylor PA, Seidlitz J, Sponheim C, Perkins P, Ungerleider LG, Glen D, Messinger A. 2021. A comprehensive macaque fMRI pipeline and hierarchical atlas. NeuroImage. 235:117997. doi:10.1016/j.neuroimage.2021.117997.
Keller SS, Crow T, Foundas A, Amunts K, Roberts N. 2009. Broca's area: Nomenclature, anatomy, typology and asymmetry. Brain and Language. 109(1):29–48. doi:10.1016/j.bandl.2008.11.005.
Kelly AMC, Uddin LQ, Biswal BB, Castellanos FX, Milham MP. 2008. Competition between functional brain networks mediates behavioral variability. NeuroImage. 39(1):527–537. doi:10.1016/j.neuroimage.2007.08.008.
Kolling N, Scholl J, Chekroud A, Trier HA, Rushworth MFS. 2018. Prospection, Perseverance, and Insight in Sequential Behavior. Neuron. 99(5):1069-1082.e7. doi:10.1016/j.neuron.2018.08.018.
Kouneiher F, Charron S, Koechlin E. 2009. Motivation and cognitive control in the human prefrontal cortex. Nat Neurosci. 12(7):939–945. doi:10.1038/nn.2321.
Loh KK, Hadj-Bouziane F, Petrides M, Procyk E, Amiez C. 2018. Rostro-Caudal Organization of Connectivity between Cingulate Motor Areas and Lateral Frontal Regions. Front Neurosci. 11:753. doi:10.3389/fnins.2017.00753.
Loh KK, Procyk E, Neveu R, Lamberton F, Hopkins WD, Petrides M, Amiez C. 2020. Cognitive control of orofacial motor and vocal responses in the ventrolateral and dorsomedial human frontal cortex. Proc Natl Acad Sci USA. 117(9):4994–5005. doi:10.1073/pnas.1916459117.
Lopez-Persem A, Verhagen L, Amiez C, Petrides M, Sallet J. 2019. The Human Ventromedial Prefrontal Cortex: Sulcal Morphology and Its Influence on Functional Organization.

J Neurosci. 39(19):3627–3639. doi:10.1523/JNEUROSCI.2060-18.2019.
von Luxburg U. 2007. A Tutorial on Spectral Clustering. [accessed 2024 Feb 26]. http://arxiv.org/abs/0711.0189.
Lv P, Xiao Y, Liu B, Wang Y, Zhang X, Sun H, Li F, Yao L, Zhang W, Liu L, et al. 2016. Dose-dependent effects of isoflurane on regional activity and neural network function: A resting-state fMRI study of 14 rhesus monkeys. Neuroscience Letters. 611:116–122. doi:10.1016/j.neulet.2015.11.037.
McKinney W. 2010. Data Structures for Statistical Computing in Python. Austin, Texas. p. 56–61. [accessed 2024 Feb 26]. https://conference.scipy.org/proceedings/scipy2010/mckinney.html.
Menzies L, Chamberlain SR, Laird AR, Thelen SM, Sahakian BJ, Bullmore ET. 2008. Integrating evidence from neuroimaging and neuropsychological studies of obsessive-compulsive disorder: The orbitofronto-striatal model revisited. Neuroscience & Biobehavioral Reviews. 32(3):525–549. doi:10.1016/j.neubiorev.2007.09.005.
Morecraft RJ, McNeal DW, Stilwell-Morecraft KS, Gedney M, Ge J, Schroeder CM, Van Hoesen GW. 2007. Amygdala interconnections with the cingulate motor cortex in the rhesus monkey. J of Comparative Neurology. 500(1):134–165. doi:10.1002/cne.21165.
Murphy K, Birn RM, Handwerker DA, Jones TB, Bandettini PA. 2009. The impact of global signal regression on resting state correlations: Are anti-correlated networks introduced? NeuroImage. 44(3):893–905. doi:10.1016/j.neuroimage.2008.09.036.
Neubert F-X, Mars RB, Sallet J, Rushworth MFS. 2015. Connectivity reveals relationship of brain areas for reward-guided learning and decision making in human and monkey frontal cortex. Proc Natl Acad Sci USA. 112(20). doi:10.1073/pnas.1410767112. [accessed 2024 Feb 26]. https://pnas.org/doi/full/10.1073/pnas.1410767112.
Palomero-Gallagher N, Mohlberg H, Zilles K, Vogt B. 2009. Cytology and receptor architecture of human anterior cingulate cortex. J of Comparative Neurology. 508(6):906–926. doi:10.1002/cne.21684.
Passingham RE, Stephan KE, Kötter R. 2002. The anatomical basis of functional localization in the cortex. Nat Rev Neurosci. 3(8):606–616. doi:10.1038/nrn893.
Patriat R, Birn RM, Keding TJ, Herringa RJ. 2016. Default-Mode Network Abnormalities in Pediatric Posttraumatic Stress Disorder. Journal of the American Academy of Child & Adolescent Psychiatry. 55(4):319–327. doi:10.1016/j.jaac.2016.01.010.
Paus T. 2001. Primate anterior cingulate cortex: Where motor control, drive and cognition interface. Nat Rev Neurosci. 2(6):417–424. doi:10.1038/35077500.
Pedregosa F, Varoquaux G, Gramfort A, Michel V, Thirion B, Grisel O, Blondel M, Prettenhofer P, Weiss R, Dubourg V, et al. Scikit-learn: Machine Learning in Python. MACHINE LEARNING IN PYTHON.
Petrides M, Cadoret G, Mackey S. 2005. Orofacial somatomotor responses in the macaque monkey homologue of Broca's area. Nature. 435(7046):1235–1238. doi:10.1038/nature03628.
Phillips ML, Drevets WC, Rauch SL, Lane R. 2003. Neurobiology of emotion perception II: implications for major psychiatric disorders. Biological Psychiatry. 54(5):515–528. doi:10.1016/S0006-3223(03)00171-9.
Picard N, Strick PL. 1996. Motor Areas of the Medial Wall: A Review of Their Location and Functional Activation. Cereb Cortex. 6(3):342–353. doi:10.1093/cercor/6.3.342.
Posner J, Song I, Lee S, Rodriguez CI, Moore H, Marsh R, Blair Simpson H. 2016. Increased functional connectivity between the default mode and salience networks in unmedicated adults with obsessive-compulsive disorder: Default Mode and Salience Networks in OCD. Hum Brain Mapp. 38(2):678–687. doi:10.1002/hbm.23408.
Procyk E, Wilson CRE, Stoll FM, Faraut MCM, Petrides M, Amiez C. 2016. Midcingulate Motor Map and Feedback Detection: Converging Data from Humans and Monkeys. Cereb Cortex.:bhu213. doi:10.1093/cercor/bhu213.
Raichle ME, MacLeod AM, Snyder AZ, Powers WJ, Gusnard DA, Shulman GL. 2001. A default mode of brain function. Proc Natl Acad Sci USA. 98(2):676–682. doi:10.1073/pnas.98.2.676.
Rakic P. 1988. Specification of Cerebral Cortical Areas. Science. 241(4862):170–176. doi:10.1126/science.3291116.
Régis J, Mangin J-F, Ochiai T, Frouin V, Riviére D, Cachia A, Tamura M, Samson Y. 2005. "Sulcal Root" Generic Model: a Hypothesis to Overcome the Variability of the Human Cortex Folding Patterns. Neurol Med Chir(Tokyo). 45(1):1–17. doi:10.2176/nmc.45.1.
Rizzolatti G, Luppino G. 2001. The Cortical Motor System. Neuron. 31(6):889–901. doi:10.1016/S0896-6273(01)00423-8.
Saberi M, Khosrowabadi R, Khatibi A, Misic B, Jafari G. 2021. Topological impact of negative links on the stability of resting-state brain network. Sci Rep. 11(1):2176. doi:10.1038/s41598-021-81767-7.
Schaeffer DJ, Gilbert KM, Ghahremani M, Gati JS, Menon RS, Everling S. 2018. Intrinsic functional clustering of anterior cingulate cortex in the common marmoset. NeuroImage. 186:301–307. doi:10.1016/j.neuroimage.2018.11.005.
Schaeffer DJ, Hori Y, Gilbert KM, Gati JS, Menon RS, Everling S. 2020. Divergence of rodent and primate medial frontal cortex functional connectivity. Proc Natl Acad Sci USA. 117(35):21681–21689. doi:10.1073/pnas.2003181117.
Schlag J, Schlag-Rey M. 1987. Evidence for a supplementary eye field. Journal of Neurophysiology. 57(1):179–200. doi:10.1152/jn.1987.57.1.179.
Seidlitz J, Sponheim C, Glen D, Ye FQ, Saleem KS, Leopold DA, Ungerleider L, Messinger A. 2018. A population MRI brain template and analysis tools for the macaque. NeuroImage. 170:121–131. doi:10.1016/j.neuroimage.2017.04.063.
Shenhav A, Botvinick MM, Cohen JD. 2013. The Expected Value of Control: An Integrative Theory of Anterior Cingulate Cortex Function. Neuron. 79(2):217–240. doi:10.1016/j.neuron.2013.07.007.
Sun L, Cao Q, Long X, Sui M, Cao X, Zhu C, Zuo X, An L, Song Y, Zang Y, et al. 2012. Abnormal functional connectivity between the anterior cingulate and the default mode network in drug-naïve boys with attention deficit hyperactivity disorder. Psychiatry Research: Neuroimaging. 201(2):120–127. doi:10.1016/j.pscychresns.2011.07.001.
Vogt BA. 2005. Pain and emotion interactions in subregions of the cingulate gyrus. Nat Rev Neurosci. 6(7):533–544. doi:10.1038/nrn1704.
Vogt BA. 2016. Midcingulate cortex: Structure, connections,

homologies, functions and diseases. Journal of Chemical Neuroanatomy. 74:28–46. doi:10.1016/j.jchemneu.2016.01.010.

Vogt BA, Berger GR, Derbyshire SWG. 2003. Structural and Functional Dichotomy of Human Midcingulate Cortex. Eur J Neurosci. 18(11):3134–3144.

Vogt BA, Nimchinsky EA, Vogt LJ, Hof PR. 1995. Human cingulate cortex: Surface features, flat maps, and cytoarchitecture. J of Comparative Neurology. 359(3):490–506. doi:10.1002/cne.903590310.

Vogt BA, Vogt L, Laureys S. 2006. Cytology and functionally correlated circuits of human posterior cingulate areas. NeuroImage. 29(2):452–466. doi:10.1016/j.neuroimage.2005.07.048.

Wang H, Fan J. 2007. Human Attentional Networks: A Connectionist Model. Journal of Cognitive Neuroscience. 19(10):1678–1689. doi:10.1162/jocn.2007.19.10.1678.

Weissenbacher A, Kasess C, Gerstl F, Lanzenberger R, Moser E, Windischberger C. 2009. Correlations and anticorrelations in resting-state functional connectivity MRI: A quantitative comparison of preprocessing strategies. NeuroImage. 47(4):1408–1416. doi:10.1016/j.neuroimage.2009.05.005.

White L. 1997. Structure of the human sensorimotor system. I: Morphology and cytoarchitecture of the central sulcus. Cerebral Cortex. 7(1):18–30. doi:10.1093/cercor/7.1.18.

Whitfield-Gabrieli S, Fischer AS, Henricks AM, Khokhar JY, Roth RM, Brunette MF, Green AI. 2018. Understanding marijuana's effects on functional connectivity of the default mode network in patients with schizophrenia and co-occurring cannabis use disorder: A pilot investigation. Schizophrenia Research. 194:70–77. doi:10.1016/j.schres.2017.07.029.